THE ASTROPHYSICAL JOURNAL, 515:42–49, 1999 April 10

ROSSI X-RAY TIMING EXPLORER HARD X-RAY OBSERVATION OF ABELL 754: CONSTRAINING THE HOTTEST TEMPERATURE COMPONENT AND THE INTRACLUSTER MAGNETIC FIELD

AZITA VALINIA,[1,2] MARK J. HENRIKSEN,[3] MICHAEL LOEWENSTEIN,[1,2] KURT ROETTIGER,[4]
RICHARD F. MUSHOTZKY,[1] AND GREG MADEJSKI[1,2]

Received 1998 August 25; accepted 1998 November 18

ABSTRACT

Abell 754, a cluster undergoing merging, was observed in hard X-rays with the *Rossi X-Ray Timing Explorer* (*RXTE*) in order to constrain its hottest temperature component and search for evidence of nonthermal emission. Simultaneous modeling of *RXTE* data and those taken with previous missions yields an average intracluster temperature of ~ 9 keV in the 1–50 keV energy band. A multitemperature component model derived from numerical simulations of the evolution of a cluster undergoing a merger produces similar quality of fit, indicating that the emission measure from the very hot gas component is sufficiently small that it renders the two models indistinguishable. No significant nonthermal emission was detected. However, our observations set an upper limit of 7.1×10^{-14} ergs cm^{-2} s^{-1} keV^{-1} (90% confidence limit) to the nonthermal emission flux at 20 keV. Combining this result with the radio synchrotron emission flux, we find a lower limit of 0.2 μG for the intracluster magnetic field. We discuss the implications of our results for the theories of magnetic field amplifications in cluster mergers.

Subject headings: galaxies: clusters: individual (Abell 754) — intergalactic medium — magnetic fields — X-rays: galaxies

1. INTRODUCTION

Clusters of galaxies are known to contain a large fraction of their mass in the form of X-ray–emitting gas in the temperature range 10^7–10^8 K. The primary X-ray emission from the intracluster medium (ICM) is thermal bremsstrahlung and line emission due to this hot diffuse gas. However, the possibility that some of the emission may be nonthermal has been raised in the past (e.g., Bridle & Feldman 1972; Harris & Romanishin 1974). The most likely mechanism for nonthermal emission in the ICM is inverse Compton (IC) scattering of cosmic microwave background (CMB) photons off relativistic (GeV) intracluster electrons. The presence of such energetic electrons is even more likely within galaxy clusters that are known to have significant radio emission, as it is suggested that the same relativistic electron population produces the synchrotron emission. As a result, the power-law slope of the nonthermal X-ray emission and that of the synchrotron radio emission are expected to be the same. Whereas very high energy electrons with short lifetimes are required for synchrotron radio emission, lower energy electrons can scatter CMB photons up to X-ray energies (Felten & Morrison 1966). For an electron with energy $E = \gamma m_e c^2$, where $\gamma(>1000)$ is the Lorentz factor, the final frequency of a CMB photon (ν_b) after scattering off the energetic electron will be (e.g., Pacholczyk 1970)

$$\nu_x = \frac{4\gamma^2 \nu_b}{3} . \quad (1)$$

Combining the X-ray inverse Compton and the radio synchrotron emission fluxes, a lower limit to the magnetic field and an upper limit to the energy density of relativistic electrons can be derived *independent* of equipartition or equal-energy hypotheses. Deriving a lower limit for the mean value of the magnetic field in the ICM is particularly important for at least two reasons. First, it affects total mass and baryonic fraction estimates of the cluster because of the possibility of extra magnetic pressure support. This has important consequences for the underlying cosmological model and estimating the value of the cosmological parameter Ω. For example, in the core of A2218 the X-ray mass estimate, under the assumption that the gas is supported by thermal pressure *alone*, is lower than the gravitational lensing estimate by a factor of 2.5 ± 0.5. It has been suggested that nonthermal pressure support is a plausible explanation for the discrepancy (Loeb & Mao 1994). Second, detection of nonthermal emission and estimates of magnetic field strength have important implications for cooling flows, since the presence of the field can suppress conduction and affect cooling of the gas. Incidentally, we point out that it has been suggested that the luminous extreme-ultraviolet (EUV) emission recently discovered in clusters of galaxies is also a result of inverse Compton scattering of CMB radiation by low-energy cosmic-ray electrons ($\gamma \sim 300$) in the intracluster medium (Sarazin & Lieu 1998). These particles have been suggested to be a relic population of cosmic rays produced by nonthermal activity over the lifetime of the cluster.

Aside from exploring nonthermal emission in clusters and deriving limits on the ICM magnetic fields and relativistic electron energy density, hard X-ray observations are needed in the study of clusters that show evidence of extremely high temperatures. There is ample evidence that a component of extremely hot gas exists in some clusters (e.g., A754) that cannot be explained by the depth of the gravitational potential (Henriksen & Markevitch 1996; Roettiger, Stone, & Mushotzky 1998b). Such hard X-ray emission could be the result of hydrodynamic processes such as

[1] Laboratory for High Energy Astrophysics, Code 662, NASA/Goddard Space Flight Center, Greenbelt, MD 20771; valinia@milkyway.gsfc.nasa.gov.
[2] Department of Astronomy, University of Maryland, College Park, MD 20742.
[3] Physics Department, University of North Dakota, Grand Forks, ND 58202.
[4] Department of Physics and Astronomy, University of Missouri, Columbia, MO 65211.

shocks. Many clusters are believed to have formed through merger events as predicted in hierarchical large-scale structure models. As a result, due to the collision of subclumps and merging effects, very high temperature shocked gas can be produced in the ICM.

There is evidence that A754, a rich cluster of galaxies at $z = 0.054$, is a merger in progress. The X-ray emission is offset significantly from the bimodal galaxy distribution. Furthermore, the intracluster medium is found to be nonisothermal (Henriksen & Markevitch 1996). Its X-ray morphology is asymmetric and not centered on the galaxy distribution. Our goal in observing this cluster with *RXTE* is twofold. One purpose is to constrain the hottest temperature component of its ICM using high-energy data. This complements the softer X-ray studies with *ASCA* and provides further constraints for numerical models of cluster evolution that, in turn, are necessary to constrain the underlying physical processes in the ICM. The second goal is to search for evidence of nonthermal emission in the integrated spectrum from the cluster and to constrain the magnetic field and relativistic electron energy density in the ICM.

The plan of this paper is as follows. In § 2 we review the derivation of magnetic field and relativistic electron energy density limits from radio and X-ray observations. In § 3 we describe the X-ray observations and the data reduction procedure. In § 4 we present the results of the analysis. This includes results of spectral analysis using both isothermal and multitemperature models (constructed from numerical simulations), and constraints on nonthermal emission. In § 5 we discuss the implications of these results and present our conclusions.

2. NONTHERMAL X-RAY EMISSION AND IMPLICATIONS FOR THE INTRACLUSTER MAGNETIC FIELD STRENGTH

Nonthermal X-ray emission in the intracluster medium is expected to arise as a result of the boosting of CMB photons to X-ray energies from scattering off relativistic electrons. This process is more likely in clusters with diffuse radio halos, since synchrotron radiation can be produced by this same population of relativistic electrons traversing the ICM magnetic field. From synchrotron emission alone, it is difficult to decouple the relativistic electron density from the magnetic field strength without invoking the equipartition hypothesis. On the other hand, the electron spectrum can be derived from the X-ray emission produced via inverse Compton scattering by energetic electrons of CMB photons, independent of the knowledge of the magnetic field. The radio synchrotron emission measurement can then be used to derive limits on both the magnetic field strength and the electron energy density averaged along the line of sight. Detailed calculations are given, for example, in Harris & Romanishin (1974), Harris & Grindlay (1979), and Rephaeli (1977a, 1977b) with many of the fundamental formulae given in Pacholczyk (1970). Here, following Henriksen (1998), we review this technique from fundamental arguments.

The number density of relativistic electrons in the ICM can be described by a power-law distribution

$$N(\gamma) = N_0 \gamma^{-p}, \quad \gamma_{\min} \le \gamma \le \gamma_{\max}, \tag{2}$$

where γ is the electron Lorentz factor, and N_0 is the amplitude coefficient. For this electron distribution, the synchrotron and inverse Compton emission fluxes are given by (using eqs. [6.36] and [7.31] of Rybicki & Lightman 1979)

$$F_s(\nu_r) = \frac{N_0 K_1 R_h^3}{3D^2} B^{(p+1)/2} \nu_r^{(1-p)/2} \tag{3}$$

and

$$F_c(\epsilon_x) = \frac{N_0 K_2 R_h^3}{3D^2} (kT)^{(p+5)/2} \epsilon_x^{(1-p)/2}, \tag{4}$$

respectively, where ν_r is the frequency of the radio photons and ϵ_x is the energy of the X-ray photons. R_h is the radius of the radio halo, D is the distance to the cluster, B is the magnetic field component perpendicular to the line of sight, k is the Boltzmann constant, and T is the temperature of the CMB radiation. K_1 and K_2 are given by

$$K_1 = \frac{\sqrt{3}\, q^3}{mc^2(p+1)} \Gamma\left(\frac{p}{4} + \frac{19}{12}\right) \Gamma\left(\frac{p}{4} - \frac{1}{12}\right) \left(\frac{2\pi mc}{3q}\right)^{(1-p)/2} \tag{5}$$

and

$$K_2 = \frac{8\pi^2 r_0^2}{h^3 c^2} J(p) \Gamma\left(\frac{p+5}{2}\right) \zeta\left(\frac{p+5}{2}\right), \tag{6}$$

respectively, where q is the electron charge, m is the electron mass, c is the speed of light, r_0 is the classical electron radius, Γ is the gamma function, ζ is the Riemann zeta function defined by

$$\zeta \equiv \sum_{n=1}^{\infty} n^{-s}, \tag{7}$$

and $J(p)$ is given by

$$J(p) = 2^{p+3} \frac{p^2 + 4p + 11}{(p+3)^2(p+5)(p+1)}. \tag{8}$$

These calculations assume that the electron distribution is isotropic and that $\gamma_{\min}^2 \ll \nu_r/\nu_B \ll \gamma_{\max}^2$, where $\nu_B \equiv qB/2\pi m_e c$ is the gyrofrequency in the magnetic field. The observed radio spectrum is given by a power-law function of the form

$$F_s(\nu_r) = A \nu_r^{-\alpha_r}, \tag{9}$$

where α_r is the energy spectral index and is equal to the X-ray spectral index α_x. It is also related to the electron power-law index, p, via the relation $p = 1 + 2\alpha_r$. Since equation (4) can be independently solved for N_0, the relativistic electron energy density and magnetic field component perpendicular to the line of sight can then be found from

$$\rho_e = N_0 \int_{\gamma_{\min}}^{\gamma_{\max}} (\gamma mc^2) \gamma^{-p} \, d\gamma \tag{10}$$

and

$$B = \left(\frac{3AD^2}{K_1 N_0 R_h^3}\right)^{2/(p+1)}, \tag{11}$$

respectively. If the inverse Compton X-ray emission flux is only an upper limit, the above equations yield an upper limit for ρ_e and a lower limit for B.

3. OBSERVATIONS AND DATA ANALYSIS

3.1. *X-Ray Observations*

A754 was observed with the proportional counter array (PCA) and the High Energy X-Ray Timing Experiment

(HEXTE) instruments on board *RXTE* during 1997 December for a total duration of 70 ks. The PCA (Jahoda et al. 1996) has a total collecting area of 6500 cm^2, an energy range of 2–60 keV, and energy resolution of $\sim 18\%$ at 6 keV. The collimator field of view is approximately circular (2° diameter) with FWHM of 1°. The HEXTE (Rothschild et al. 1998) consists of two clusters, each having a collecting area of 800 cm^2, an energy range of 15–250 keV, energy resolution of 15% at 60 keV, and a field of view of 1° FWHM. Furthermore, each cluster "rocks" along mutually orthogonal directions to provide background measurements away from the source.

We used the most recent PCA background estimator program PCABACKEST (Version 2.0c; L7 model) provided by the *RXTE* Guest Observer Facility (GOF) to estimate the background. In addition to the intrinsic instrument background and the cosmic X-ray background (CXB), additional counts are induced via Southern Atlantic Anomaly (SAA) passages. A754 observations were performed during non-SAA orbits, and therefore the activation-induced background was estimated to be zero by PCABACKEST.

We used the data taken when all five detectors of the PCA were on and the elevation angle from the limb of the Earth was greater than 10°. This reduced the good time interval for the purpose of analysis to ~ 60 ks. For this time duration, the background-subtracted count rate over the 3–20 keV band was 41.04 ± 0.0399 counts s^{-1}. The background-subtracted count rate over the 15–50 keV energy band was 0.3363 ± 0.0728 counts s^{-1} and 0.3515 ± 0.0607 counts s^{-1} for HEXTE clusters A and B, respectively. The total on-source integration time for the HEXTE detectors was 20 ks.

X-ray images of A754 from the *ROSAT* position sensitive proportional counter (PSPC) archive indicate that the radio galaxy 26W20, a member of the cluster, lies in the field of view of *RXTE*. Since one of the goals of our investigation is to search for evidence of nonthermal emission in the ICM, we need to investigate the contribution of this galaxy to the integrated nonthermal emission from the cluster. The PSPC data, obtained in 1992 November, reveal this source to be approximately 40′ from the center of A754, with a spectrum that is well described as a power law with a hydrogen column density of $(6.6 \pm 0.08) \times 10^{20}$ cm^{-2} and a photon index of 2.0 ± 0.2. The 0.5–2 keV flux of this source is 2.5×10^{-12} ergs cm^{-2} s^{-1}, with a nominal 10% error. With this spectrum, the 2–10 keV flux would correspond to $\sim 3.8 \times 10^{-12}$ ergs cm^{-2} s^{-1}, a factor of ~ 30 smaller than the integrated flux of A754 in the same band. Furthermore, at the position of the source in the field of view of PCA, the transmission is only about a third of the full response at the center of the field of view. Therefore, we conclude that the contribution of 26W20 to the total integrated flux from A754 (particularly in the 2–10 band) is negligible and does not affect the temperature determination of this cluster. On the other hand, the 10–40 keV flux of this galaxy would correspond to $\sim 3 \times 10^{-12}$ ergs cm^{-2} s^{-1}. Since only about a third of this flux will get transmitted through the collimator, its contribution in the 10–40 keV band will be $\sim 10^{-12}$ ergs cm^{-2} s^{-1}. We discuss its effect on the detection of nonthermal IC radiation in § 4.3.

In addition to *RXTE* data, we have extracted *Ginga* LAC and *ASCA* GIS2 spectra from archival observations of this cluster with exposure times of 10 and 20 ks, respectively. The background-subtracted count rate for the LAC over the 3–18 keV range was 20.24 ± 0.0719 counts s^{-1}, while for the GIS2 over 1–10 keV it was 1.687 ± 0.0095counts s^{-1}. In § 4 we present results from simultaneous fits to the spectra in the 1–50 keV band obtained from all four instruments.

3.2. *Radio Observations*

The 2.7 GHz data presented by Andernach et al. (1988) for the extended radio source they associate with a possible diffuse (12′) halo in A754 has a flux density of 137 mJy. The synchrotron flux can then be written as $F_s = 2.5 \times 10^{-12} \nu^{-1.3}$ ergs s^{-1} cm^{-2} Hz^{-1}, where we have used the value $\alpha_r = 1.3$ reported by Mills, Hunstead, & Skellern (1978) and Jaffe & Rudnick (1979) at 408 and 610 MHz, respectively, since it is expected that the lowest frequency data should have the least contamination from discrete radio sources. The 1.4 GHz data of Mills et al. (1978), and more recently Condon et al. (1998) (NRAO/VLA Sky Survey [NVSS]) show that at least three discrete sources can be resolved in the extended halo (these are sources 6, 7, and 8 in Fig. 1*a* of Mills et al. 1978). At least one of these sources has been identified as a narrow-angle tail (NAT) radio galaxy by Zhao et al. (1989) and Owen & Ledlow (1997). These three NVSS sources have flux densities of 58.0, 98.9, and 20.4 mJy, respectively, at 1.4 GHz. Using the Andernach et al. (1988) flux at 2.7 GHz and a spectral index of $\alpha_r = 1.3$ for the extended source, the expected flux density at 1.4 GHz is 322 mJy. Subtracting the flux density of the combined three discrete sources from the total flux at 1.4 GHz yields a flux density of approximately 145 mJy which may be attributed to the diffuse emission. The synchrotron flux for the diffuse radio emission can then be written as

$$F_s = 1.1 \times 10^{-12} \nu^{-1.3} \text{ ergs s}^{-1} \text{ cm}^{-2} \text{ Hz}^{-1} . \quad (12)$$

We will use this flux relation in § 4.3 to estimate a lower limit for the magnetic field and an upper limit for the relativistic electron energy density.

4. RESULTS

4.1. *Isothermal Model*

We first attempt to fit the A754 spectrum with the redshifted, optically thin collisional ionization equilibrium plasma model of Raymond & Smith (1977). For comparison purposes, we first fit the spectra from *RXTE* PCA, *Ginga* LAC, and *ASCA* GIS2 independently over the 3–10 keV range (the overlapping energy band in all three instruments) with an isothermal model. Table 1 summarizes the fit parameters and the field of view of each instrument. Note that A754 has a diameter of approximately 0°.5, and fits within the field of view of all the above-mentioned instruments. Reassuringly, the fitting results are consistent for all instruments within their respective error bars.

We then fit the PCA/LAC/GIS2/HEXTE spectra simultaneously in the 1–50 keV energy band. Figure 1 shows the results of the fit, while Table 2 summarizes the best-fit parameters. The fit is satisfactory and the derived average temperature of ~ 9 keV is consistent (within error bars) with the temperature derived from each individual instrument. It is also consistent with the emissivity-weighted average temperature previously derived using *ASCA* data (Henriksen & Markevitch 1996). The simultaneous PCA/HEXTE fit also yields similar results within error bars (although the error bars are larger than the ones quoted in Table 2).

TABLE 1

ISOTHERMAL MODEL FIT OVER 3–10 keV ENERGY RANGE

Instrument	FOV (FWHM)	kT	Abundance	$\chi^2(\nu)$
RXTE PCA[a]	1°	9.06 ± 0.13	0.177 ± 0.012	21.8(15)
Ginga LAC	1° × 2°	9.26 ± 0.28	0.18 ± 0.03	11.2(9)
ASCA GIS	40′ diameter	10.93 ± 2.1	0.23 ± 0.09	327.8(333)

[a] Because of the residual xenon L-edge at ≈4 keV in the detector's response, 0.004 counts s^{-1} systematic error was added to the spectrum to obtain a reduced χ^2 below 2 for the fit.

4.2. *Multitemperature Model*

We have considered a multitemperature model based on three-dimensional numerical simulations of A754 (Roettiger, Stone, & Mushotzky 1998b). The intracluster medium is evolved using an Eulerian hydrodynamics code based on the piecewise parabolic method (PPM), and the collisionless dark matter is evolved via an N-body particle-mesh (PM) code. In the simulations, two clusters are allowed to merge under the influence of their mutual gravity, having been given an initial relative velocity of 270 km s^{-1} parallel to the line connecting the centers of the two subclusters and 100 km s^{-1} perpendicular to this direction. This results in a slightly off-axis merger with an impact parameter of ∼120 kpc and a final impact velocity of ∼2500 km s^{-1}. Roettiger et al. (1998b) find that the epoch that most closely represents A754 occurs ∼0.3 Gyr after the closest approach of the respective centers of mass.

Figure 2*a* shows the fractional distribution (by volume) of gas at a given temperature within a 2 Mpc box centered on the X-ray emission. The cooler peak (at ∼6.5 keV) represents the initial primary cluster temperature. All gas hotter than ∼7 keV has been heated by the merger. In particular, the extended high-temperature tail is the result of a shock along the leading edge of one of the subclusters to the northwest. Figure 2*b* shows the fractional distribution of the emission measure of the gas at a given temperature within the same region described for panel *a*. The two peaks in (*a*) have merged into one near 7.5 keV. The effective emission-weighted temperature within this region is ∼9 keV, similar to that derived from observations.

We implemented this model by summing a series of redshifted multitemperature Raymond-Smith (1977) plasma components of fixed temperature and relative emission measure following that presented in Figure 2*b*, and fitted the data allowing the column density N_H and metal abundance—assumed identical for all temperature components—to vary. The goodness of fit ($\chi^2 = 712.0$ for 636 dof) to the simultaneous *RXTE*/*ASCA*/*Ginga* data for this model is slightly poorer but comparable to that of the isothermal model. The best-fit hydrogen column density and abundances for this model are also similar, $(0.10 \pm 0.02) \times 10^{22}$ cm^{-2} and 0.183 ± 0.006 solar, respectively. Essentially, this model is indistinguishable from the isothermal model in moderate energy resolution integrated X-ray spectra. This point can be further illustrated in Figure 3, where we have plotted the expected flux for the isothermal (*dashed line*) and multitemperature (*solid line*) models, respectively, using the PCA response function. The two models are nearly indistinguishable up to about 15 keV. Above 20 keV the difference in the hard tail widens. However, at 40 keV, the multitemperature model differs from the isothermal model flux by approximately 8×10^{-14} ergs cm^{-2} s^{-1} keV^{-1}. This difference is smaller than $\sim 4 \times 10^{-13}$ ergs cm^{-2} s^{-1} keV^{-1} or the fluctuations on cosmic X-ray background (CXB) per *RXTE* beam at 40 keV. Since any high-temperature gas present in the cluster, as predicted in numerical merger simulations, has a small emission measure compared to that of the bulk of the gas, the integrated spectra of the two models are indistinguishable with current instruments.

TABLE 2

BEST-FIT PARAMETERS FOR THE ISOTHERMAL MODEL OVER 1–50 keV ENERGY RANGE: SIMULTANEOUS FITS FOR *ASCA*/*Ginga*/PCA/HEXTE

Parameter	Value
N_H[a] [atom cm^{-2} (10^{22})]	0.08 ± 0.02
kT	8.98 ± 0.06
Abundance	0.174 ± 0.006
RXTE PCA normalization	0.0997 ± 0.0004
RXTE HEXTE A/PCA cross-normalization[b]	0.72 ± 0.1
RXTE HEXTE B/PCA cross-normalization[b]	0.61 ± 0.12
ASCA GIS/PCA cross-normalization[b]	1.04 ± 0.02
Ginga LAC/PCA cross-normalization[b]	0.84 ± 0.009
χ^2(dof)	659.9(634)

[a] Galactic value in the direction of A754 is 0.045.

[b] Instrument normalization can be obtained by multiplying this number by the PCA normalization.

4.3. *Constraints on Nonthermal Emission and the Magnetic Field*

To constrain the nonthermal emission in hard X-rays, we fit the *RXTE* data (PCA and HEXTE) with an isothermal plus a power-law model. We assumed that the power-law photon index in the X-ray model is that obtained from the radio observations (§ 3.2). To model the contribution of 26W20 in the field of view (40′ away from the center as discussed in § 3.1), we included a fixed power-law component of photon index 2 with a flux of $\sim 10^{-12}$ ergs cm^{-2} s^{-1} in the 10–40 keV band. At the 90% confidence limit, the combined thermal plus power-law fit to the data gives only an upper limit of $\sim 4.9 \times 10^{-14}$ ergs cm^{-2} s^{-1} keV^{-1} for the nonthermal flux at 20 keV. Integrated over the 10–40 keV band, the flux upper limit is $\sim 1.4 \times 10^{-12}$ ergs cm^{-2} s^{-1}. At the 99.7% confidence limit (or 3 σ level), the above upper limits increase to $\sim 1.2 \times 10^{-13}$ and 3.5×10^{-12} ergs cm^{-2} s^{-1} keV^{-1}, respectively.

The above result neglects the effect of CXB fluctuations in the spectrum. However, these fluctuations have been determined to be about 8% rms of the mean CXB (Gruber 1998, private communication) per *RXTE* field of view. Using the energy flux (in units of keV cm^{-2} s^{-1} keV^{-1} sr^{-1})

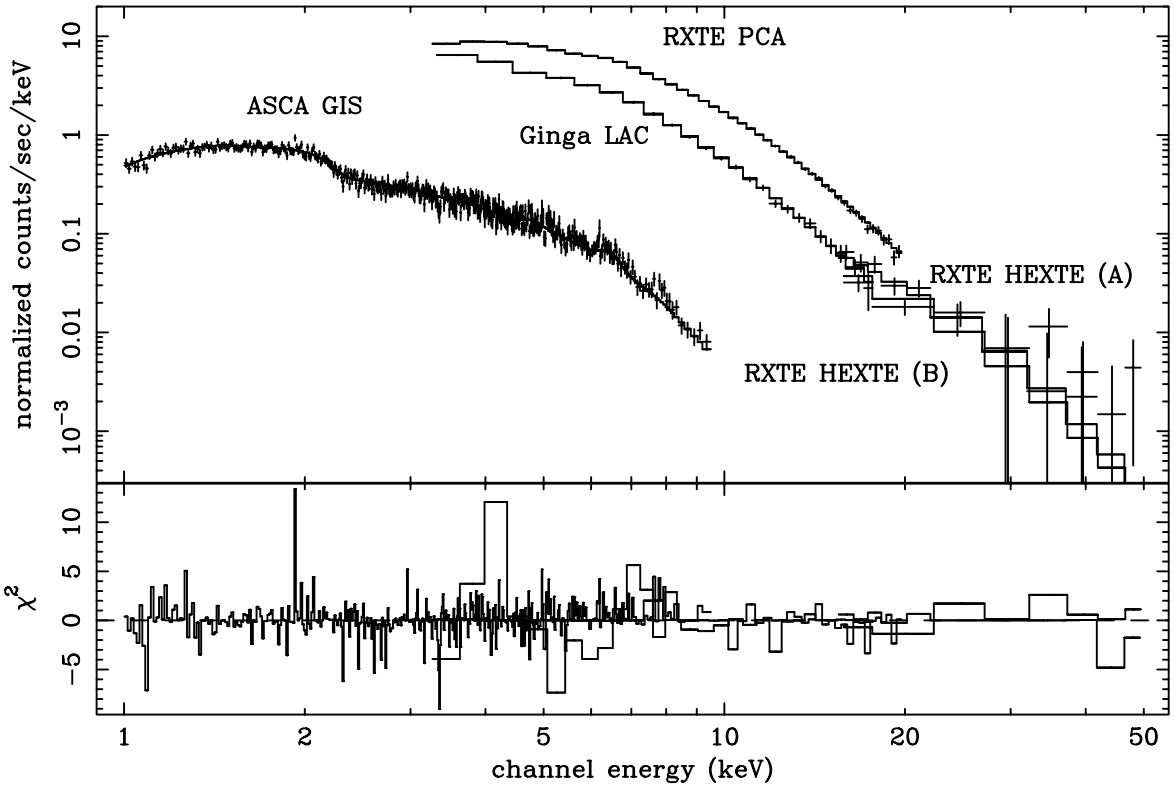

FIG. 1*a*

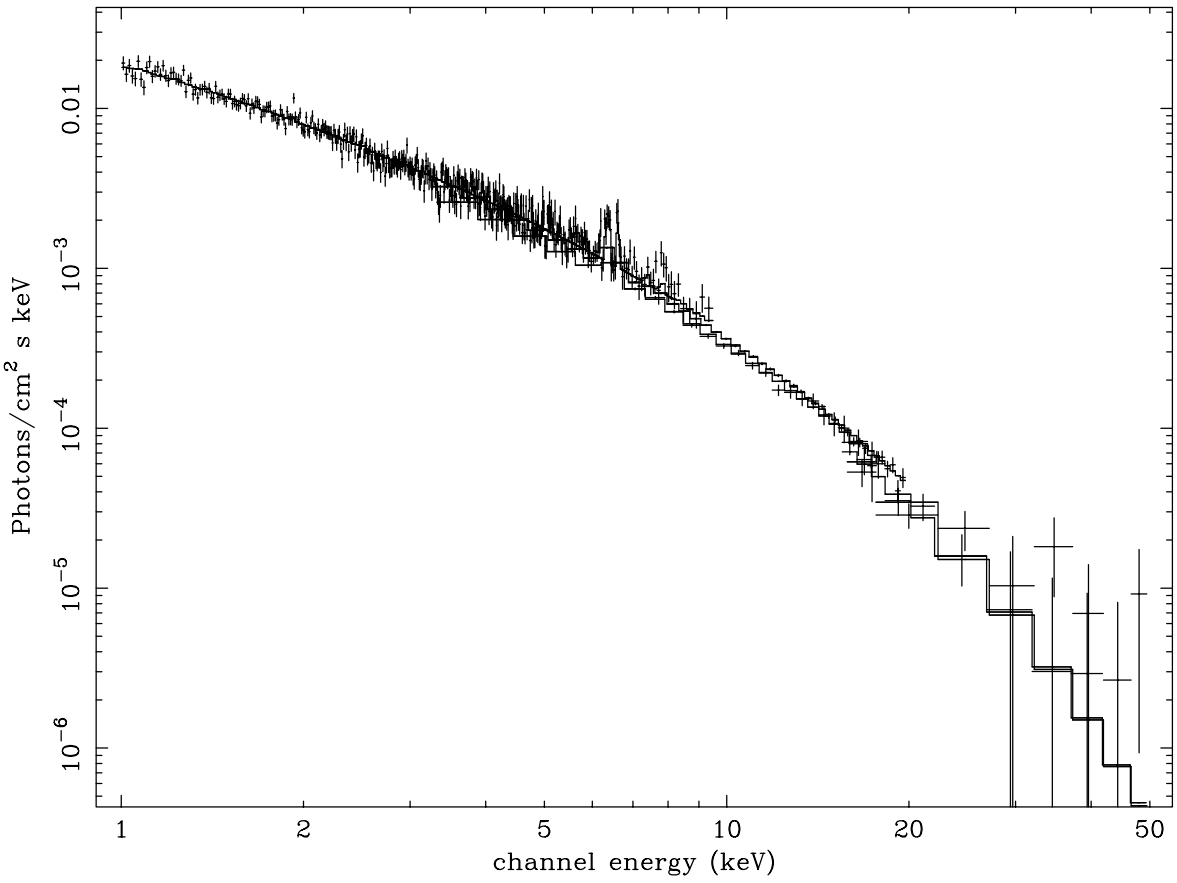

FIG. 1*b*

FIG. 1.—(*a*) Simultaneous fit to PCA/HEXTE/GIS/LAC data over the 1–50 keV band with an isothermal model (best-fit parameters given in Table 2). (*b*) Same as (*a*), except that the unfolded spectrum is shown.

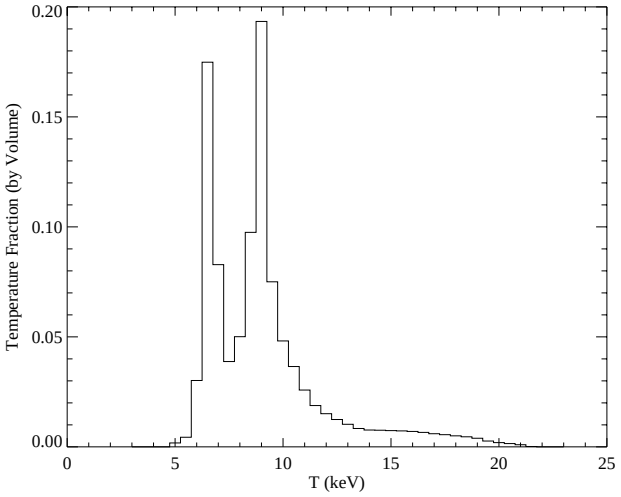

FIG. 2*a*

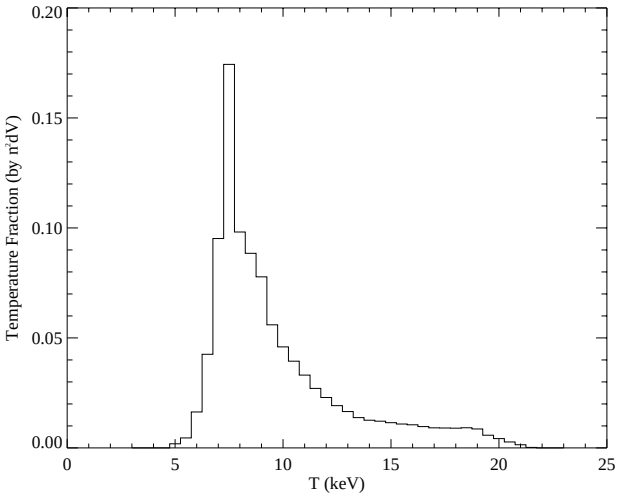

FIG. 2*b*

FIG. 2.—(*a*) Fractional distribution (by volume) of gas at a given temperature within a 2 Mpc box centered on the X-ray emission. The cooler peak represents the initial primary cluster temperature. All gas hotter than ~ 7 keV has been heated by the merger. (*b*) Fractional distribution (weighted by differential emission measure $n^2\,dV$) of gas at a given temperature within the same region described in (*a*). The two peaks in (*a*) have merged into one near 7.5 keV. The effective emission-weighted average temperature within this region is ~ 9 keV.

$$F(E) = 7.9E^{-0.29} \exp\left(-\frac{E}{41.13 \text{ keV}}\right), \quad 3 \text{ keV} < E < 60 \text{ keV}, \quad (13)$$

for the CXB (Gruber 1992), the fluctuation amplitude amounts to 6.5×10^{-14} ergs cm^{-2} s^{-1} keV^{-1} per *RXTE* field of view at 20 keV. Since this value is comparable to the nonthermal upper limit derived for A754, the effect of CXB fluctuations on modeling of the data cannot be neglected.

To determine a more accurate upper limit, we modeled the fluctuation spectrum by equation (13) and fixed its amplitude in our spectral modeling. At the 90% confidence limit, a positive full amplitude fluctuation (i.e., 8% of the CXB) yields an upper limit of $\sim 3.6 \times 10^{-14}$ ergs cm^{-2} s^{-1} keV^{-1} for the nonthermal flux at 20 keV and an integrated flux of $\sim 10^{-12}$ ergs cm^{-2} s^{-1} in the 10–40 keV band. At the 99.7% confidence limit, the above upper limits

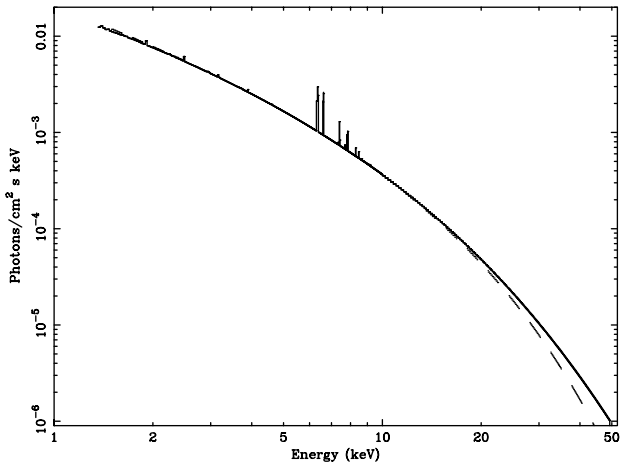

FIG. 3.—Expected spectrum of isothermal (*dashed line*) and multitemperature (*solid line*) models described in §§ 4.1 and 4.2 using the PCA response matrix.

increase to $\sim 10^{-13}$ and 2.8×10^{-12} ergs cm^{-2} s^{-1}, respectively. At the 90% confidence limit, a negative amplitude fluctuation yields $\sim 7.1 \times 10^{-14}$ ergs cm^{-2} s^{-1} keV^{-1} and $\sim 2 \times 10^{-12}$ ergs cm^{-2} s^{-1} for the flux at 20 keV and the 10–40 keV integrated flux, respectively. At the 99.7% confidence limit, the above upper limits increase to $\sim 1.6 \times 10^{-13}$ and 4.4×10^{-12} ergs cm^{-2} s^{-1}, respectively.

To find a lower limit on B and an upper limit on ρ_e, we solve equation (4) for N_0 by using the upper-limit inverse Compton flux over the 10–40 keV energy band. We use the 90% confidence limits to derive limits on B and ρ_e. Since our upper limit to the 10–40 keV flux is in the range $(1\text{–}2) \times 10^{-12}$ ergs cm^{-2} s^{-1}, an upper limit of $(1.4\text{–}2.8) \times 10^{-3}$ cm^{-3} is derived for N_0.

The detection of nonthermal X-ray photons at energy E_X primarily samples electrons of energy $\gamma = (3E_X/4h\nu_b)^{1/2}$, where ν_b is the CMB photon frequency, and m_e and c are the electron rest mass and the speed of light, respectively.

Integrating equation (10) over the 10–40 keV range using the upper-limit flux derived over this band, we find an upper limit of $(1.1\text{–}2.2) \times 10^{-15}$ ergs cm^{-3} for the relativistic electron energy density in the intracluster medium. Equation (11) yields a lower limit of 0.2–0.27 μG for the magnetic field strength.

Note that the electron energy range over which we integrated equation (10) corresponds to radio emission in the range 16–64 MHz ($E = \gamma m_e c^2 = (\nu_r/c_0\,B)^{1/2}$; $c_0 = 6.27 \times 10^{18}$), which is the frequency of maximum synchrotron emission (Pacholczyk 1970). Our calculations, therefore, assume that the radio spectrum extends down to 16 MHz with the same spectral index. We note that from simultaneous analysis of *HEAO 1* and *ASCA* data, Henriksen (1998) finds a lower limit of 0.29 μG for this cluster.

5. DISCUSSION AND CONCLUSIONS

We have presented X-ray observations and data analysis of Abell 754, a cluster in the process of a merger event. In addition to the newly obtained *RXTE* PCA/HEXTE data, we obtained archival *ASCA* GIS and *Ginga* LAC data of this cluster and simultaneously fitted the spectra from all four instruments. We found that the integrated spectrum of the whole cluster in the 1–50 keV energy band can be fitted well with an isothermal collisional ionization equilibrium

plasma model (Raymond & Smith 1977) of temperature ~ 9 keV, consistent within the error bars with previous temperature measurements of this cluster.

We then fitted the data with a multitemperature model derived from numerical simulations of two merging subclusters with conditions similar to those found in Abell 754 (Roettiger et al. 1998b). The average emission-weighted temperature from the simulations was ~ 9 keV, similar to that found from observations. In this model, the emission measure from the very hot gas, shock heated in the merger, is relatively small. As a result, this model produces a fit to the data of similar quality to that of the isothermal model. Calculation of the resultant spectrum from the two models indicates that the two spectra are nearly indistinguishable below ~ 15 keV, and it is only above 20 keV that the hard X-ray tails from the two models depart. However, the difference between the two models at 40 keV is less than $\sim 10^{-13}$ ergs cm^{-2} s^{-1} keV^{-1}, lower than the amplitude of the CXB fluctuations at that energy per *RXTE* field of view. Hence, the two models are indistinguishable with the obtained *RXTE* spectrum.

To search for evidence of nonthermal emission from the cluster, we added a power law to the isothermal model with the photon index fixed at the value obtained for the radio emission power law. No significant nonthermal emission was found. However, the *RXTE* data imply an upper limit (90% confidence limit) of $\sim(3.6\text{–}7.1) \times 10^{-14}$ ergs cm^{-2} s^{-1} keV^{-1} for the nonthermal flux at 20 keV, where the lower and upper numbers are those derived assuming a full positive and negative CXB fluctuation amplitude, respectively, as discussed in § 4.3. Using the upper-limit flux integrated over the 10–40 keV band and the radio emission data from Andernach et al. (1988), we find an upper limit of $(1.1\text{–}2.2) \times 10^{-15}$ ergs cm^{-3} for the relativistic electron energy density and a lower limit of 0.2–0.27 μG for the magnetic field strength in the intracluster medium, where the given ranges represent the inclusion of positive and negative CXB fluctuations.

The magnetic field would have to be 2 orders of magnitude greater than this lower limit in order for the average magnetic pressure to be comparable to the average thermal pressure in the hot gas. In regions of higher than average density where the field would be expected to be compressed to higher values, the thermal pressure is enhanced by a comparable factor. Therefore, there is no evidence for dynamically important magnetic fields in A754.

The upper limit to the magnetic field derived assuming energy equipartition of the magnetic field with the relativistic electrons is 0.17–0.23 μG, below (or comparable to) the lower-limit field strength derived from combining radio and X-ray observations (depending on the unknown level of the CXB fluctuations for that region of the sky). If it is the case that the equipartition field is lower than that observed, one interpretation is that since A754 is undergoing a merger, magnetic fields are being amplified in the merger process and the ensuing turbulence. This interpretation has been confirmed in numerical simulations of cluster mergers where the field is observed to be amplified by several factors in localized regions (Roettiger, Stone, & Burns 1998a). Unfortunately, it is difficult to draw any firm conclusions regarding the relation between the equipartition value and the actual strength of the magnetic field in A754 based on the available data. Higher resolution VLA 90 cm radio images of the extended emission and higher spatial resolution X-ray images (e.g., with *AXAF*) are needed to make more definitive statements.

There have been several lines of speculation on magnetic field generation in the ICM. One school of thought is that galactic wakes power a dynamo (e.g., Jaffe 1980; Roland 1981). However, as shown by Goldman & Rephaeli (1991) and De Young (1992), galactic wakes do not adequately produce the observed fields. It has been suggested that more powerful sources such as cluster mergers could be responsible (e.g., De Young 1992). Since both magnetic field amplification and reacceleration of energetic particles are expected in cluster mergers from the resulting shocks and turbulence, large-scale radio halos are likely to be formed around these clusters. However, while the magnetic reconnection time in the intracluster medium,

$$t_{\rm rec} \approx 2 \times 10^9 \left(\frac{\epsilon}{0.1}\right)^{-1} \left(\frac{l_t}{1\ {\rm kpc}}\right) \left(\frac{B}{\mu{\rm G}}\right)^{-1} \left(\frac{n_p}{0.1\ {\rm cm}^{-3}}\right)^{1/2} {\rm yr}\ , \quad (14)$$

is long (where the reconnection proceeds with an average velocity of ϵv_A and $\epsilon \approx 0.1$; Soker & Sarazin 1990), the inverse Compton energy loss time given by

$$t_{\rm IC} = \frac{\gamma m_e c^2}{(4/3)\sigma_{\rm T} c \gamma^2 U_{\rm CMB}} \approx 4.8 \times 10^8 \left(\frac{\gamma}{4800}\right)^{-1} {\rm yr} \quad (15)$$

for an electron of energy ~ 20 keV ($\gamma \approx 4800$) is comparatively short. This may be the underlying reason for radio halos to be a transient phenomenon and the fact that they are usually associated with cluster mergers or dynamically young clusters (Tribble 1993). This association has also been noted by Edge, Stewart, & Fabian (1992) and Watt et al. (1992).

The ultimate origin of the magnetic fields in clusters is still debatable. Suggestions have been made that magnetic field and relativistic particles in clusters originate within cluster radio sources and are dispersed into the intracluster medium during merger events (Tribble 1993; Harris et al. 1993). Finally, we note that the recent discovery of EUV emission in clusters of galaxies and its possible origin as inverse Compton scattering of CMB photons off low-energy cosmic-ray electrons indicate that old radio halos should be present in a large number of clusters, albeit at very low frequencies that are not detectable from Earth.

This research has taken advantage of HEASARC and LEDAS archival databases.

REFERENCES

Andernach, H., Tie, H., Sievers, A., Reuter, H.-P., Junkes, N., & Wielebinski, R. 1988, A&AS, 73, 265
Bridle, A. H., & Feldman, P. A. 1972, Nature Phys. Sci., 235, 168
Condon, J. J., Cott, W. D., Greisen, E. W., Yin, Q. F., Perley, R. A., Taylor, G. B., & Broderick, J. J. 1998, AJ, 115, 1693
De Young, D. S. 1992, ApJ, 386, 464
Edge, A. C., Stewart, G. C., & Fabian, A. C. 1992, MNRAS, 258, 177
Felten, F. E., & Morrison, P. 1966, ApJ, 146, 686
Goldman, I., & Rephaeli, Y. 1991, ApJ, 380, 344
Gruber, D. E. 1992, in The X-Ray Background, ed. X. Barcons & A. C. Fabian (New York: Cambridge Univ. Press), 44
Harris, D. E., & Grindlay, J. 1979, MNRAS, 188, 25
Harris, D. E., & Romanishin, W. 1974, ApJ, 188, 209
Harris, D. E., Stern, C. P., Willis, A. G., & Dewdney, P. E. 1993, AJ, 105, 769
Henriksen, M. J. 1998, PASJ, in press

Henriksen, M. J., & Markevitch, M. L. 1996, ApJ, 466, L79
Jaffe, W. 1980, ApJ, 241, 925
Jaffe, W., & Rudnick, L. 1979, ApJ, 233, 453
Jahoda, K., Swank, J. H., Giles, A. B., Stark, M. J., Strohmayer, T., Zhang, W., & Morgan, E. H. 1996, Proc. SPIE, 2808, 59
Loeb, A., & Mao, S., 1994, ApJ, 435, L109
Mills, B., Hunstead, R., & Skellern, D. 1978, MNRAS, 185, 51
Owen, F. N., & Ledlow, M. J. 1997, ApJS, 108, 41
Pacholczyk, A. G. 1970, Radio Astrophysics (San Francisco: Freeman)
Raymond, J. C., & Smith, B. W. 1977, ApJS, 35, 419
Rephaeli, Y. 1977a, ApJ, 212, 608
———. 1977b, ApJ, 218, 323
Roettiger, K., Stone, J. M., & Burns, J. O. 1998a, ApJ, submitted
Roettiger, K., Stone, J. M., & Mushotzky, R. F. 1998b, ApJ, 493, 62
Roland, J. 1981, A&A, 93, 407
Rothschild, R. E., et al. 1998, ApJ, 496, 538
Rybicki, G., & Lightman, A. 1979, Radiative Processes in Astrophysics (New York: Wiley)
Sarazin, C. L., & Lieu, R. 1998, ApJ, 494, L177
Soker, N., & Sarazin, C. 1990, 348, 73
Tribble, P. C. 1993, MNRAS, 263, 31
Watt, M. P., Ponman, T. J., Bertram, D., Eyles, C. J., Skinner, G. K., & Willmore, A. P. 1992, MNRAS, 258, 738
Zhao, J.-H., Burns, J. O., & Owen, F. N. 1989, AJ, 98, 64